J Mater Sci (2007) 42:2090–2096
DOI 10.1007/s10853-006-1238-6

Preparation of $BaTiO_3$-based ceramics by nanocomposite doping process

Bo Li · Shuren Zhang · Xiaohua Zhou · Sheng Wang · Zhu Chen

Received: 13 September 2005 / Accepted: 3 February 2006 / Published online: 9 December 2006

Abstract $BaTiO_3$-based ultrafine nonreducible dielectrics for multilayer ceramic capacitors were prepared by a newly developed nanocomposite doping process. According to TG-DTA, XRD and TEM analysis, the nanocomposite dopants via sol–gel method were uniform and well dispersive. The micromechanism was investigated based on comparing conventional process with nano-doping process. It indicated that due to the special nano-effect, doping effect of additives became more effective and the microstructure and dielectric properties of ceramics were improved. The results showed that high performance dielectrics satisfying X8R specification were achieved, with high dielectric constant of 2,900, low dielectric loss of 0.6% and large insulation resistivity of 10^{12} Ω cm.

Introduction

The future developments in high performance multilayer ceramic capacitors (MLCCs), driven by the market requirements, are miniaturization, high volumetric efficiency, high reliability and low manufacturing costs. Keys to achieve the goal are to develop high dielectric constant materials, reduce the thickness of dielectric layers and simultaneously increase the number of stacked layers, as well as to utilize inexpensive internal electrodes and terminations. Today, MLCCs with over 700 dielectric layers of below 2 μm thickness have been developed. Therefore, it is most important and critical to research and develop ultrafine dielectrics in MLCCs industry [1].

In recent years, many studies have been performed on $BaTiO_3$-based temperature-stable nonreducible dielectric materials, which satisfy X7R or even X8R specifications [1–4]. This is achieved by forming the so-called grain core-shell structure in $BaTiO_3$ ceramics. This chemically inhomogeneous structure consists of ferroelectric unreacted grain core and paraelectric modified grain shell [1, 4]. Hydrothermally synthesized $BaTiO_3$ powders are employed widely because the powders have controlled powder morphology, fine particle size, low agglomeration, and require no calcination, in comparison with other methods, such as solid-state reaction, sol–gel technique and coprecipitation method [5–8]. For the conventional solid-state method, small amount of various additives with different particle size are usually mechanically mixed with the matrix powders. Consequently, large particles of the additives may induce local segregation of the additives in the dielectric layers and cause an initial loss of the insulation resistance of MLCCs. The distribution of the additives in the matrix become critical, when many fine $BaTiO_3$ particles are associated with a low doping level of coarse particle additives. Instead of solid-state mixing, chemical mixing techniques such as sol–gel coating, precipitation coating and solution coating can be effective in enhancing the mixed homogeneity of minor constituents [9–11]. However, these coating methods are restricted in the industry manufacture of MLCCs

B. Li (✉) · S. Zhang · X. Zhou · S. Wang · Z. Chen
School of Microelectronics and Solid-State Electronics, University of Electronic Science and Technology of China, Chengdu, Sichuan 610054, P.R. China
e-mail: lbuestc@163.com

because of the disadvantages, such as complicated process and high production cost. To overcome the disadvantages above, a new nanocomposite doping process (nano-doping process) has been developed in our previous research [12], which can be effective in controlling the particle size of additives and enhancing the mixed homogeneity of minor constituents. The nanocomposite dopants (nano-dopants) is prepared by sol–gel method using cheap raw material, and then added into matrix, which acts as grain growth inhibitor, shifter, depressor and sintering aid to achieve the acceptable temperature characteristics.

In this work, $BaTiO_3$-based ultrafine nonreducible ceramics satisfying X8R specification for Ni-MLCCs was prepared by the nano-doping process successfully. The effect of nano-dopants on the microstructure and dielectric properties of $BaTiO_3$ ceramics was studied. Especially, the nano-doping micromechanism was further investigated based on comparing conventional process with nano-doping process.

Experimental procedure

Sample preparation

The aqueous precursor solutions containing yttrium nitrate ($Y(NO_3)_3$, A.R.) and magnesium nitrate ($Mg(NO_3)_2$, A.R.) were dissolved in ethanol (C_2H_5OH, A.R.) and ethyl silicate ($Si(OC_2H_5)_4$, TEOS, C.P.) under vigorous stirring. Transparent sols could be obtained after complete hydrolysis reaction and transform to transparent gels by drying at 60 °C for 12 h. Then xerogels were acquired by heating the wet gels at 100 °C for several days. After calcining and milling, the nano-dopants were achieved. The molar ratio of Y, Mg and Si elements in the nano-dopants is 3:2:1.

Hydrothermally synthesized $BaTiO_3$ (Ba/Ti = 1.00) with an average particle size of 0.4 μm was employed. The sample Nano was prepared by the following nano-doping process. Nano-dopants (2 wt%) were added to the fine $BaTiO_3$ matrix. In comparison with sample Nano, the sample Conv was prepared by the conventional solid-state mixing process. Reagent grade submicron Y_2O_3, MgO and SiO_2 with average particle size of 0.4, 0.3 and 0.7 μm, respectively, were used as additives to $BaTiO_3$. The concentration of Y, Mg and Si elements were equal to those in the nano-dopants. Subsequently, both raw mixtures were wet ball-milled for 6 h, respectively, using deionized water and ZrO_2 balls, and then dried and sieved. The obtained powders with 5 wt% PVA binder were pressed into disks with 10 mm in diameter and 1 mm thickness. After the binder was burned out at 600 °C in air, the disk samples were painted Ni paste on both surfaces and then sintered in a tube furnace at 1,260 °C for 3 h in a reducing atmosphere ($P_{O_2} = 10^{-10}$ Pa) controlled by N_2, H_2, O_2 and H_2O.

Analysis and measurement

The xerogels were investigated by the thermogravimetric and differential thermal analyses (TG-DTA, TA DSC2910) at an air flow rate of 50 mL/min and a constant heating rate of 5 °C/min from 30 to 1,200 °C. The morphologies of nano-dopants were observed by transmission electron microscopy (TEM, JEM-100CX) at 80 kV. The nano-dopants and the ceramics, after crushed and ground into powder, were characterized via X-ray diffraction (XRD, Philips X′ Pert Pro MPD), using Cu $K\alpha_1$ X-ray of wavelength 1.54056 Å with a scan step of 0.02°. Microstructures of the sintered ceramics were observed by scanning electron microscope (SEM, Hitachi S-530) with an accelerating voltage of 25 kV. Temperature dependence of dielectric properties was measured from –55 to 150 °C using a LCR automatic testing meter at 1 kHz with 1 Vrms. The dielectric constant and dielectric loss were also carried out by the LCR meter and insulation resistance was determined by a high-resistance meter in 1 min after applying 100 Vdc at room temperature.

Results and discussion

Characterization of nano-dopants

Figure 1 shows the TG-DTA curves of the xerogels within the temperature range of 30–1,200 °C. From TG

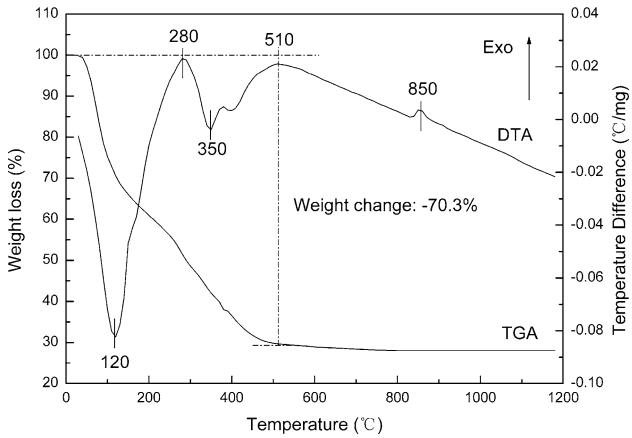

Fig. 1 TG-DTA curves of xerogels

curve, a major weight loss about 70.3% is observed below 510 °C and there is no weight loss above 700 °C. From DTA curve, there are two endothermic peaks and three exothermic peaks. The endothermic peak at 120 °C is due to the removal of hydration water and organic solvent. The next exothermic peak at 280 °C is attributed to the decomposition of nitrates and hydrated silica, as well as combustion of organic species. The endothermic peak at 350 °C is connected to the decomposition of hydrolytic polymer and formation of MgO, Y_2O_3. The two exothermic peaks located at 510 and 850 °C, respectively, are caused by the formation of amorphous composite oxides and the crystallization of composites. It can be concluded that the xerogels would totally decompose when heating up to 750 °C.

According to the results of TG-DTA, the xerogels were calcined at 750 and 950 °C for 2 h, respectively, and their XRD patterns are illustrated in Fig. 2. Single broad peak appears around 33 ° for the nano-dopants calcined at 750 °C, which indicates the formation of amorphous composite expressed as $3Y_2O_3{\cdot}4MgO{\cdot}2SiO_2$. Further increase of the calcining temperature makes the diffraction peaks sharp and strong, as a result of both the improvement of crystallinity and grain growth. The sharp diffraction peaks appear distinctly for the nano-dopants calcined at 950 °C, which coincides with the exothermic peak at 850 °C on DTA curve. This indicates that the nano-dopants changes from amorphous to crystalline phase with increase of calcining temperature.

The morphologies of obtained nano-dopants observed by TEM are shown in Fig. 3. The particles of nano-dopants calcined at 750 and 950 °C are uniform and spheroidal, with an average particle size of 40.2 and 67.9 nm, respectively. However, slight growth and agglomeration of particles are also detected when nano-dopants calcined at 950 °C. Hence, a relative lower calcining temperature of 750 °C must be adopted to achieve well dispersive and ultrafine nano-dopants.

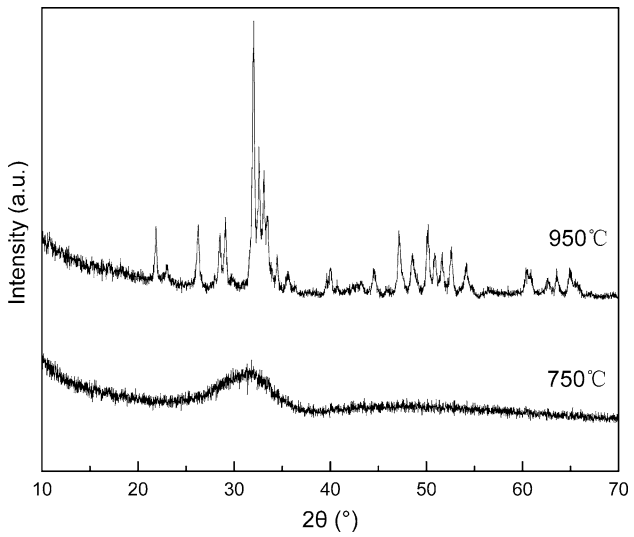

Fig. 2 XRD patterns of nano-dopants calcined at different temperatures

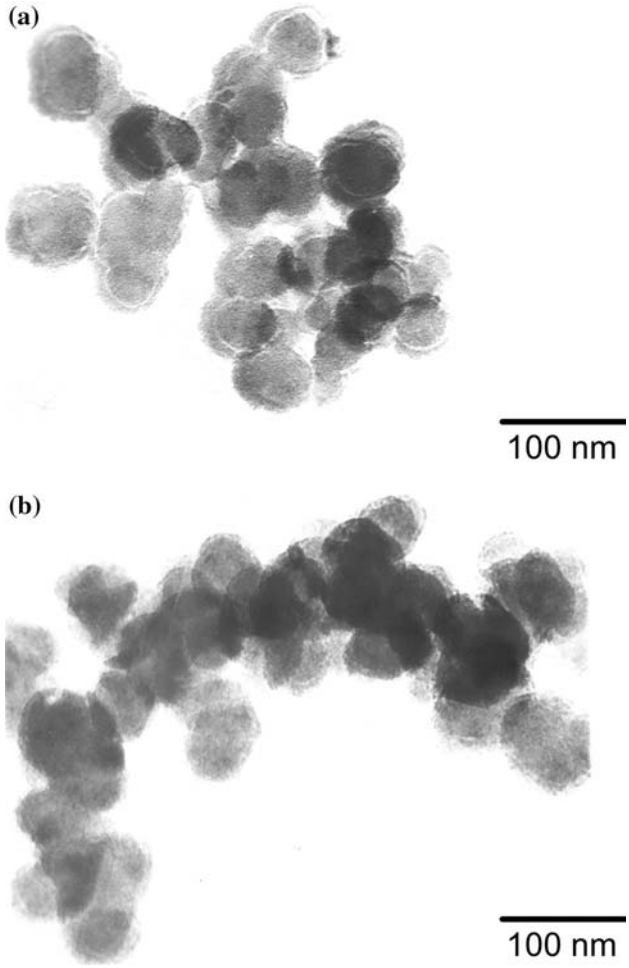

Fig. 3 TEM micrographs of nano-dopants calcined at (**a**) 750 °C, (**b**) 950 °C

Microstructure and dielectric properties

Figure 4 shows the SEM micrographs of sintered ceramics prepared by conventional and nano-doping process. Coarse grains (~1.0 μm) together with fine grains (~0.4 μm) are detected for sample Conv. Furthermore, a number of pores and voids in existence lead to the relatively low density (~5.63 g/cm^3). And this porous microstructure could result in the lower dielectric constant and worse reliability of MLCCs. On the contrary, sample Nano exhibits a very dense, uniform and fine-grained microstructure. The sintered

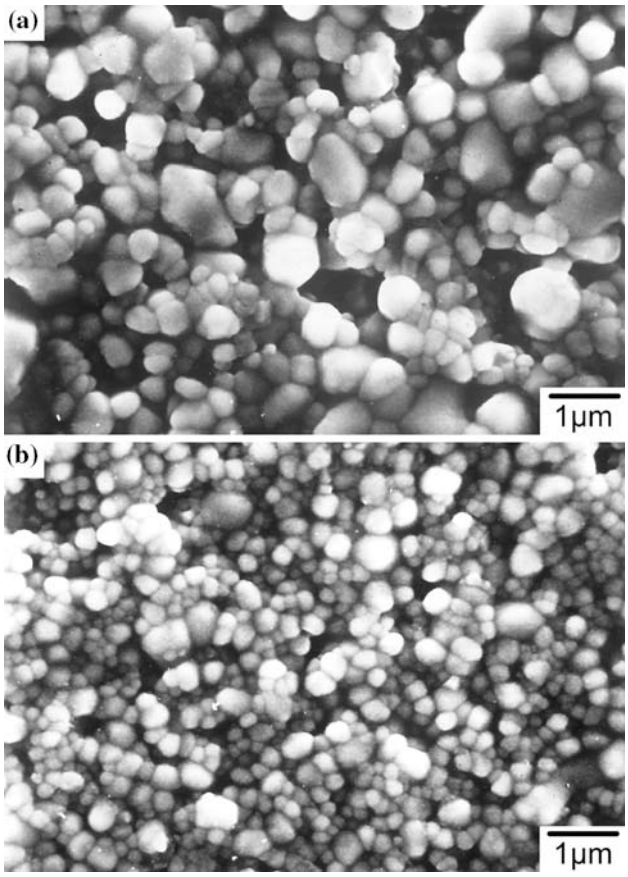

Fig. 4 SEM micrographs of sintered ceramics prepared by (**a**) conventional and (**b**) nano-doping process

density is about 5.87 g/cm^3 using Archimedes' method and the average grain size is less than 0.4 μm by the linear interception method. This illustrates that the nano-dopants could inhibit the grain growth more efficiently and be helpful to form the dense and homogeneous fine-grained ceramics. It is known that fracture toughness, IR degradation and voltage breakdown strength of MLCCs are improved as the grain size of dielectrics decrease [13–15]. Hence, the nano-doping process may be one key approach to reduce dielectric thickness and maintain good reliability of MLCCs.

Figure 5 shows the XRD patterns of the specimens prepared by conventional and nano-doping process. Within the XRD resolution limit, there is no secondary phase in existence for both cases. And we selected XRD profiles focusing on (002) and (200) diffraction peaks for determining the crystal system shown in Fig. 5. The diffraction peaks around 45° are separated from each other, corresponding to the crystal plane of (002) and (200) respectively, which indicates that the crystal structure of sample Conv is typically tetragonal. However, the two diffraction peaks are merged

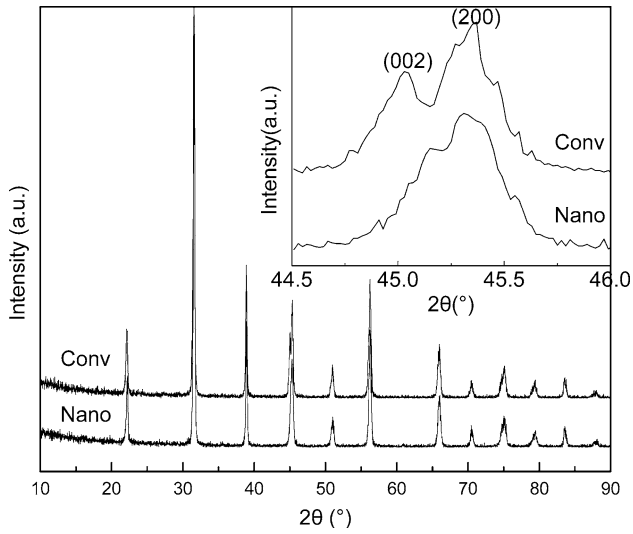

Fig. 5 X-ray analyses of specimens prepared by conventional and nano-doping process

together nearly for sample Nano. This remarkable change in the peak profile indicates that the crystal structure of sintered sample Nano is pseudocubic. According to X-ray analysis, the contraction of the *c*-axis and simultaneously slight extension of the *a*-axis are concluded. Because the grain core possesses the tetragonal structure of pure $BaTiO_3$, the tetragonality is associated with the volume fraction of grain core [16]. The tetragonality (*c*/*a* ratio) decreases, which suggests that the volume fraction of the tetragonal grain core decreases, whereas the volume fraction of the cubic grain shell increases for sample Nano.

Figure 6 shows the dielectric-temperature properties of the samples obtained from conventional and nano-doping process. In comparison with sample Conv,

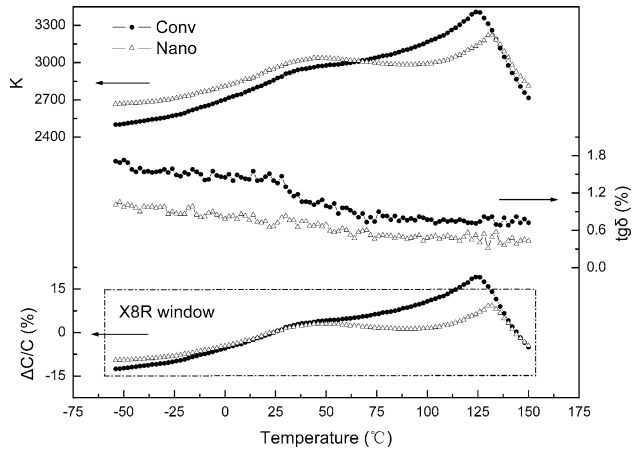

Fig. 6 Dielectric-temperature properties of samples prepared by conventional and nano-doping process

the dielectric constant peak at Curie temperature (T_C) is markedly depressed, whereas the dielectric constant at low temperatures is enhanced via nano-doping, e.g. $K_{25\ ^\circ C}$ = 2,900. Consequently, for sample Nano, the K–T curve becomes flat and the $\Delta C/C$–T characteristic is improved significantly, which satisfy the requirement of X8R specification as indicated in Fig. 6. These results could be explained by the core-shell structure theory as follows. It was confirmed that the volume fraction of grain core is responsible for the sharp dielectric constant peak intensity at T_C, while the volume fraction of grain shell is related to the broad dielectric constant peak intensity around lower temperature [16]. Thus the volume ratio of grain core to grain shell determines the dielectric-temperature behavior of the core-shell-structured $BaTiO_3$ ceramics. The above-mentioned conclusion by XRD, that the volume ratio of grain core to grain shell is increased by nano-doping as compared with conventional doping, results in a significant improvement on the K–T and $\Delta C/C$–T behavior. As shown in Fig. 6, the Curie temperature (T_C) of sample Conv is around 126 °C, which is close to that of pure $BaTiO_3$ ceramic, i.e. 125 °C, in this study. However, the T_C of sample Nano shifts up to 131 °C, which could be attributed to the increase of internal stress between the grain core and grain shell regions [18]. Moreover, it is obvious that the overall dielectric loss (tgδ) is decreased gradually with increasing temperature for both samples as illustrated in Fig. 6. The tgδ–T curve of sample Nano is nearly close to a horizontal line within the measuring temperature range. The dielectric loss at room temperature ($tg\delta_{25\ ^\circ C}$) of sample Nano (~0.6%) is much lower than that of sample Conv (~1.5%), and the insulation resistivity (IR) of sample Nano (~10^{12} Ω cm) is higher than that of sample Conv (~10^{11} Ω cm).

Micromechanism of nano-doping

Figure 7 illustrates the sketch maps of micromechanism of conventional and nano-doping process. After the mixing step, the doped dielectric powders are composed of $BaTiO_3$ matrix and additives. For conventional process, submicron size additives utilized could not distribute uniformly in $BaTiO_3$ powders. It is difficult for $BaTiO_3$ particles surrounded by the conventional additives with comparative particle size, as shown in Fig. 7a. This means that during the sintering, some $BaTiO_3$ particles do not see the additive particles and behave like the undoped $BaTiO_3$ material. Accordingly, the sintered ceramic shows an inhomogenous microstructure with large grains as shown in Fig. 4a. Simultaneously, the quantity of core-shell-structured grains (CS-grains) is also limited.

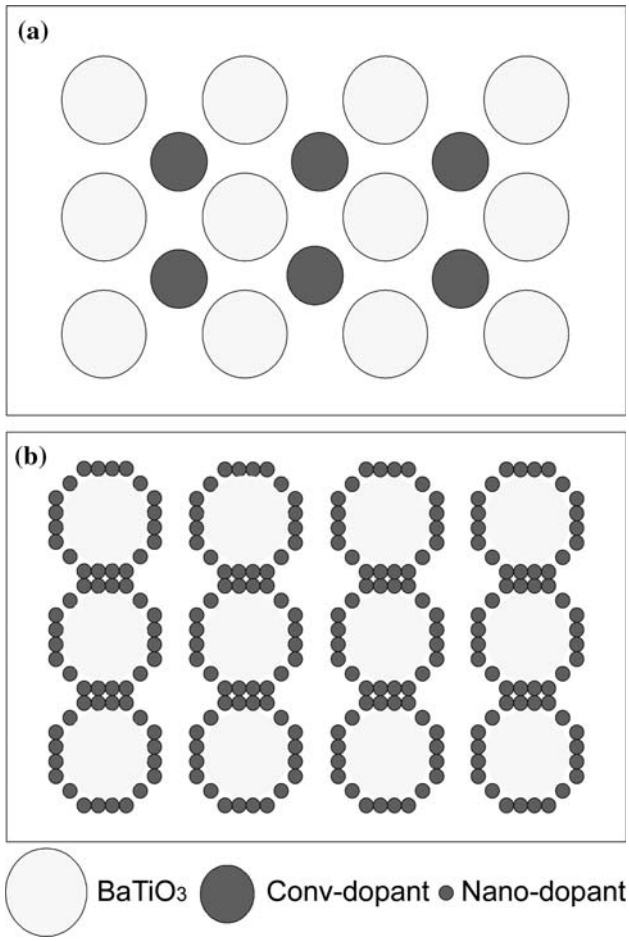

Fig. 7 Sketch map of micromechanism of (**a**) conventional and (**b**) nano-doping process

Nano-dopants, due to a relatively small particle size, are liable to distribute in $BaTiO_3$ matrix uniformly and coat the $BaTiO_3$ particles completely, as shown in Fig. 7b. Assuming that nano-dopants adsorb on the surface of $BaTiO_3$ particles, the additives such as Y_2O_3 and MgO would be well distributed along the surface of $BaTiO_3$ particles in a similar way. This modification of the surface could be the origin of the grain growth control. During sintering nano-dopants, uniformly distributed on the grain boundaries, could inhibit the grain growth effectively and promote the densification of ceramics. Thus the sintered sample Nano reveals a homogeneous fine-grained microstructure as shown in Fig. 4b. Furthermore, nano-dopants could easily diffuse into the outer regions of $BaTiO_3$ particles, which become the grain shell regions. Large amount of CS-grains could be formed when abundant $BaTiO_3$ particles coated by nano-dopants. Therefore, the uniform

distribution of nano-dopants on the surface of $BaTiO_3$ particles could be favorable to form the desired core-shell microstructure in fine-grained $BaTiO_3$ ceramics.

The atoms in the nano-dopants particles (especially the surface atoms) become more active compared with that in the submicron dopants, due to the particular characteristics of nanopowder, such as surface effect and small-scale effect (large specific surface area, high interfacial energy, and so on). So the nano-dopants could interact with $BaTiO_3$ more severely. The nano-doping ions behave a so strong tendency to be incorporated into $BaTiO_3$ lattice, that the diffusion length of nano-dopants is deeper than that of submicron dopant. The average thickness of grain shell in the ceramic by nano-doping is larger than that of conventional doping. Namely, the cubic grain shell volume increases and the tetragonality decreases, which demonstrated the above result of XRD analysis.

For the core-shell-structured ceramics, the dielectric constant can be calculated according to the Lichtenecker and Rother formula [17],

$$\ln K = V_1 \ln K_1 + V_2 \ln K_2$$

where V_1, V_2 and K_1, K_2 are the respective volume fraction and dielectric constant of the grain core and grain shell. Accordingly, low dielectric constant at T_C but high dielectric constant at low temperature is obtained by nano-doping. It is thus confirmed that the significant improvement of temperature characteristics could be ascribed to nano-doping affecting the ratio of the grain core to grain shell.

Moreover, the core-shell structure is produced by the diffusion of Y and Mg ions in $BaTiO_3$ grains, which would make the crystal lattice distorted and bring internal stress. Because the grain core is pure $BaTiO_3$, this distortion mainly occurs at the grain shell that consisted of reacted $BaTiO_3$ heavily doped with additives. As mentioned-above, for sample Nano, more doping ions are easily incorporated into the $BaTiO_3$ lattice, resulting in the severe distortion of the crystal lattice and the increase of grain shell volume. The severely mismatch between the grain core and grain shell may give rise to higher internal stress at the interface, which could shift the T_C to higher temperature and improve the temperature dependence of dielectric constant [18, 19]. Therefore, the flat dielectric-temperature characteristic with high performance, such as high K and low tgδ, is attributed to the formation of abundant core-shell-structured fine grains with relatively thicker grain shell via nano-doping. It could be concluded that doping effect of additives become more effective due to the special nano-effect, and the microstructure and dielectric properties of so acquired ceramics are improved consequently.

Conclusions

High performance $BaTiO_3$-based nonreducible dielectrics were achieved by nano-doping process, with high dielectric constant of 2,900, low dielectric loss of 0.6% and large insulation resistivity of 10^{12} Ω cm, which satisfy EIA X8R specification. TG-DTA and XRD indicated the nanocomposite changed from amorphous to crystalline phase with increase of calcining temperature. TEM showed the nano-dopants acquired by sol–gel method are uniform, spheroidal and well dispersive, with an average particle size of 40.2 nm calcined at 750 °C. It was observed that particles grew and agglomerated slightly at higher temperature. Due to the uniform ultrafine particles as well as uniformly distributing in $BaTiO_3$ matrix and coating the $BaTiO_3$ particles completely, nano-dopants could inhibit grain growth efficiently and be favorable to form desired core-shell microstructure in the fine-grained $BaTiO_3$ ceramics, with an average grain size of 0.4 μm. The flat dielectric-temperature characteristic with high performance is attributed to the formation of abundant core-shell-structured fine grains with relatively thicker grain shell via nano-doping. It could be concluded that the doping effect of additives became more effective due to the special nano-effect, and the microstructure and dielectric properties of so acquired ceramics were improved consequently.

References

1. Kishi H, Mizuno Y, Chazono H (2003) Jpn J Appl Phys 42:1
2. Zhang SR, Wang S, Zhou XH, Li B, Chen Z (2005) J Mater Sci: Mater Electron 16:669
3. Wang S, Zhang SR, Zhou XH, Li B, Chen Z (2005) Mater Lett 59:2457
4. Kishi H, Okino Y, Honda M, Iguchi Y, Imaeda M, Takahashi Y, Ohsato H, Okuda T (1997) Jpn J Appl Phys 36:5954
5. Templeton LK, Pask JA (1959) J Am Ceram Soc 42:212
6. Lemonine C, Michaux B, Pirard JP, Lecloux AJ (1994) J Non-Cryst Solids 175:1
7. Stockenhuber M, Mayer H, Lercher JA (1990) J Am Ceram Soc 76:1185
8. Kumazawa H, Kagimoto T, Kawabata A (1996) J Mater Sci 31:2599. DOI 10.1007/BF00187288
9. Kumar U, Wang SF, Selvaraj U, Dougherty JP (1994) Ferroelectrics 154:283

10. Selmi FA, Amarakoon VRW (1988) J Am Ceram Soc 71:934
11. Bruno SA, Swanson DK, Burn I (1993) J Am Ceram Soc 76:1233
12. Wang S, Zhou XH, Zhang SR, Li B, Chen Z (2005) J Mater Sci: Mater Electron 16:257
13. Zang Z, Raj R (1995) J Am Ceram Soc 78:3363
14. Waser R, Baiatu T, Hardtl KH (1990) J Am Ceram Soc 73:1645
15. Fang TT, Hsieh HL, Shiau FS (1993) J Am Ceram Soc 76:1205
16. Park Y, Kim YH, Kim HG (1996) Mater Lett 28:101
17. Lichtenecker K, Rother K (1931) Z Phys 32:255
18. Sato S, Fujikawa Y, Nomura T (2000) Am Ceram Soc Bull 79:155
19. Armstrong TR, Buchanan RC (1990) J Am Ceram Soc 73:1268